PERGAMON

International Journal of Solids and Structures 39 (2002) 3625–3647

INTERNATIONAL JOURNAL OF SOLIDS and STRUCTURES

www.elsevier.com/locate/ijsolstr

Effect of dilatancy on the strain localization of water-saturated elasto-viscoplastic soil

Fusao Oka *, Yosuke Higo, Sayuri Kimoto

Department of Civil Engineering, Kyoto University, Yoshida-honmachi, Sakyo-ku, Kyoto 606-8501, Japan

Received 13 February 2002

Abstract

It is well known that geomaterials such as soils exhibit an increase in volume during shearing deformation, referred to as dilatancy. Dilatancy is a typical property of such granular materials as soils and is closely related to changes in the microstructure. Normally consolidated clay exhibits negative dilatancy or contractancy, namely, a decrease in volume during shearing. On the other hand, overconsolidated clay shows positive dilatancy, namely, an increase in volume during shearing. The aim of the present paper is to study the effects of the microstructure, such as dilatancy and permeability, on the strain localization of water-saturated clay using an elasto-viscoplastic constitutive model. Based on the non-linear kinematic hardening theory and a Chaboche type of viscoplasticity model, an elasto-viscoplastic model for both normally consolidated and overconsolidated clays is proposed; the model can address both negative and positive dilatancies. Firstly, the instability of the model under undrained creep conditions is analyzed in terms of the accelerating creep failure. The analysis shows that clay with positive dilatancy is more unstable than clay with negative dilatancy. Secondly, a finite element analysis of the deformation of water-saturated clay is presented with focus on the numerical results under plane strain conditions. From the present numerical analysis, it is found that both dilatancy and permeability prominently affect shear strain localization behavior.

Keywords: Strain localization; Dilatancy; Two-phase mixture; Clay; Elasto-viscoplasticity

1. Introduction

The problem of strain localization in such geomaterials as soils and rocks has been studied in the context of experimental, theoretical, and numerical approaches over the last three decades. It has been found that the onset conditions for strain localization such as shear banding can be captured by a bifurcation analysis (see Rice (1976), among others). As such, numerous researchers have tried to numerically simulate shear banding in many engineering materials, including metals and geological materials (Loret and Prevost,

* Corresponding author.
E-mail address: foka@nakisuna.kuciv.kyoto-u.ac.jp (F. Oka).

0020-7683/02/$ - see front matter
PII: S0020-7683(02)00171-3

1991). Through these numerical studies, it has been realized that instability and ill-posedness might be encountered in the problem when using a rate-independent elasto-plastic model in the numerical analysis.

In general, there are three methods which can be used to overcome the above-mentioned instability. One method is to introduce rate dependency of the material through the use of an elasto-viscoplastic model or by way of regularization in the numerical analysis (Cormeau, 1975; Hughes and Taylor, 1978; Simo and Hughes, 1997). The second method is to introduce higher order strain gradients into the constitutive model (e.g. Aifantis, 1984, 1987; Mühlhaus and Aifantis, 1991; Vardoulakis and Aifantis, 1991; de Borst and Sluys, 1991; Aifantis et al., 1999 and Hutchinson, 2001). The third approach is to incorporate a Darcy type of soil–fluid interaction which can alleviate the problem of instability by delaying the onset of material instability (Rice, 1975, 1976; Loret and Prevost, 1991; Oka et al., 1995 and Schrefler et al., 1996). Loret and Prevost (1991) studied a dynamic strain localization problem of water-saturated soil using a Drucker–Prager model with positive dilatancy.

The present study deals with the behavior of clay in which the aspect of rate dependency comes naturally into the modeling. In addition, since the transport of water must be considered in the behavior of water-saturated clay, the problem is formulated within the solid–fluid two-phase theory. Oka et al. (1994, 1995, 2000a, 2000b) studied strain localization problems pertinent to water-saturated clays using a viscoplastic model. In particular, it was found that strain localization in the shear band of water-saturated clays could be simulated via a finite element analysis using an elasto-viscoplastic model with viscoplastic softening (Oka et al., 1995). However, the model used in the analysis was limited to normally consolidated clay with negative dilatancy.

It is well known that geomaterials with a particulate microstructure such as soil show an increase in volume during shearing deformation, which is called dilatancy. Normally consolidated clay exhibits a decrease in volume, i.e., negative dilatancy or contractancy. On the other hand, overconsolidated clay shows an increase in volume, i.e., positive dilatancy. The clay is called "normally consolidated clay", in the classical sense, if the present effective stress is the maximum stress it has ever experienced in its entire history. The clay is called "overconsolidated clay" if it has been subjected to an effective stress greater than the present one. An improvement to the classical definitions is such that the present stress of overconsolidated clay is less than the consolidation yield stress, while the present stress of normally consolidated clay is equal to the consolidation yield stress.

The above discussion prompts the following question. How do both positive and negative dilatancies affect strain localization phenomena? The answer lies in a detailed study that must include comprehensive comparisons between numerical predictions and experimental results. For this purpose, an elasto-viscoplastic model for water-saturated clay has been proposed in the present analysis based on a Chaboche type of viscoplastic theory (Chaboche and Rousselier, 1980) and the kinematic hardening rule with viscoplastic softening. The developed model can describe both negative and positive dilatancy characteristics. The instability of the model is examined under undrained triaxial creep conditions. The strain localization problem was numerically studied for water-saturated normally consolidated clay by Oka et al. (1995). It was found that negative dilatancy prominently affects strain localization. In the present paper, the effects of dilatancy and permeability are numerically investigated for both dilatant and contractant clays using the newly developed elasto-viscoplastic constitutive model which can be applied to both normally and overconsolidated clays. From the present numerical analysis, it is found that dilatancy characteristics play an important role in strain localization behavior.

The plan of the present paper is as follows. In Section 2, an elasto-viscoplastic constitutive model, applicable to both normally consolidated and overconsolidated clays, is proposed based on the non-linear kinematic hardening theory. In Section 3, the instability of the model under undrained triaxial conditions is then discussed. Finally, in Section 4, the finite element formulation for the deformation analysis of water-saturated clay is presented, and a discussion on the numerical results of the clay behavior under plane strain conditions, which highlights the effect of dilatancy on strain localization, follows.

2. Elasto-viscoplastic model for clay

Adachi and Oka (1982) proposed an elasto-viscoplastic model for water-saturated normally consolidated clay based on a Perzyna type of viscoplasticity theory (Perzyna, 1963) and Cam-clay model, has been applied to many practical problems and strain localization problems (Oka et al., 1995). In the present study, an elasto-viscoplastic model for both normally consolidated and overconsolidated clays, based on the kinematic hardening viscoplastic theory proposed by Chaboche and Rousselier, 1980, is developed. The model can be seen as an extension of the overstress type of viscoplastic model developed by Adachi and Oka (1982) for the behavior of normally and quasi-overconsolidated clays.

In the following, Terzaghi's effective stress concept is used for water-saturated soil because the compressibility of the pore water is effectively small, i.e.

$$\sigma_{ij} = \sigma'_{ij} + u_{\mathrm{w}}\delta_{ij} \tag{1}$$

where σ_{ij} is the total stress tensor, σ'_{ij} is the effective stress tensor, u_{w} is the pore water pressure, and δ_{ij} is Kronecker's delta. Furthermore, an additive decomposition of the total strain rate into elastic, $\dot{\varepsilon}^{e}_{ij}$, and viscoplastic, $\dot{\varepsilon}^{vp}_{ij}$, ones is assumed such that

$$\dot{\varepsilon}_{ij} = \dot{\varepsilon}^{e}_{ij} + \dot{\varepsilon}^{vp}_{ij} \tag{2}$$

Elastic strain rate $\dot{\varepsilon}^{e}_{ij}$ is given by a generalized Hooke type of law, i.e.

$$\dot{\varepsilon}^{e}_{ij} = \frac{1}{2G}\dot{S}_{ij} + \frac{\kappa}{3(1+e)\sigma'_{\mathrm{m}}}\dot{\sigma}'_{\mathrm{m}}\delta_{ij} \tag{3}$$

where S_{ij} is the deviatoric stress rate tensor, σ'_{m} is the mean effective stress, G is the elastic shear coefficient, e is the void ratio, κ is the swelling index, and the superimposed dot denotes time differentiation. Swelling index κ is determined by the slope of the volumetric loading–unloading curve of the natural logarithmic scale.

In the model, it is assumed that there is an overconsolidation (OC) boundary surface that delineates the OC region ($f_{\mathrm{b}} < 0$) from the normal consolidation region ($f_{\mathrm{b}} \geqslant 0$) (see Fig. 1). In previous papers (Adachi and Oka, 1984; Oka, 1992; Oka et al., 1999), a similar OC boundary surface was used in an elasto-plastic

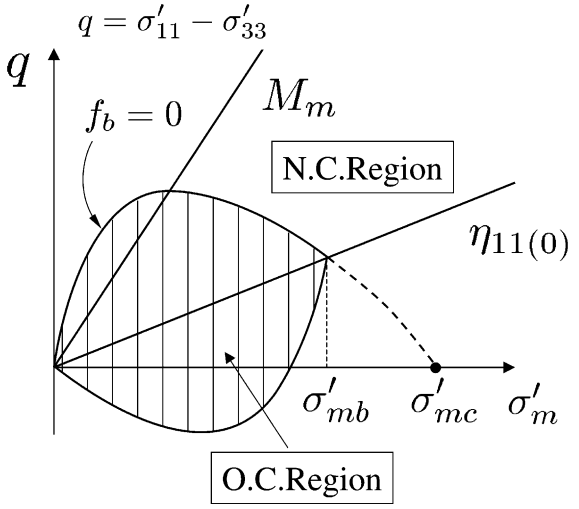

Fig. 1. Overconsolidation boundary surface under triaxial conditions.

model for sand and overconsolidated clay. The OC boundary surface was introduced to control the shape of the plastic potential function.

In order to describe the volumetric relaxation and/or secondary compression under isotropic stress conditions, it is assumed that the stress state of normally consolidated clay is generally outside of the OC boundary surface and defined as:

$$f_{\mathrm{b}} = \bar{\eta}^* + M^*_{\mathrm{m}} \ln \frac{\sigma'_{\mathrm{m}}}{\sigma'_{\mathrm{mb}}} = 0, \quad \bar{\eta}^* = \{(\eta^*_{ij} - \eta^*_{ij(0)})(\eta^*_{ij} - \eta^*_{ij(0)})\}^{1/2} \tag{4}$$

$$\sigma'_{\mathrm{mb}} = \sigma'_{\mathrm{mb}i} \exp\left(\frac{1+e}{\lambda-\kappa}\varepsilon^{vp}_{kk}\right) \tag{5}$$

$$\eta^* = \sqrt{\eta^*_{ij}\eta^*_{ij}}, \quad \eta^*_{ij} = \frac{S_{ij}}{\sigma'_{\mathrm{m}}} \tag{6}$$

$$\sigma'_{\mathrm{mc}} = \sigma'_{\mathrm{mb}} \exp\left(\frac{\eta^*_{(0)}}{M^*_{\mathrm{m}}}\right) = \sigma'_{\mathrm{mb}i} \exp\left(\frac{1+e}{\lambda-\kappa}\varepsilon^{vp}_{kk}\right) \exp\left(\frac{\eta^*_{(0)}}{M^*_{\mathrm{m}}}\right) \tag{7}$$

$$\eta^*_{(0)} = \sqrt{\eta^*_{ij(0)}\eta^*_{ij(0)}}, \quad \eta^*_{ij(0)} = \frac{S_{ij(0)}}{\sigma'_{\mathrm{m}(0)}} \tag{8}$$

in which (0) denotes the state at the end of consolidation, $\sigma'_{\mathrm{mb}i}$ is the initial value of σ'_{mb}, λ is the compression index, and M^*_{m} is the value of η^* at maximum compression. Compression index λ is determined by the slope of the volumetric loading curve of the natural logarithmic scale. In Fig. 1, $\eta_{11(0)}(=\sqrt{3/2}\eta^*_{11(0)})$ stands for the anisotropic consolidation history.

A viscoplastic flow rule is given by

$$\dot{\varepsilon}^{vp}_{ij} = C_{ijkl}\langle \Phi_1(f_{\mathrm{y}})\rangle \Phi_2(\xi)\frac{\partial f_{\mathrm{p}}}{\partial \sigma'_{kl}} \tag{9}$$

$$C_{ijkl} = a\delta_{ij}\delta_{kl} + b(\delta_{ik}\delta_{jl} + \delta_{il}\delta_{jk}), \quad C_{01} = 2b, \quad C_{02} = 3a + 2b \tag{10}$$

in which $\langle\ \rangle$ is the MacCauley's bracket; $\langle x\rangle = x$, if $x > 0$,$= 0$, if $x \leqslant 0$, C_{01}, C_{02} are viscoplastic parameters, $C_{ijkl}\langle \Phi_1(f_{\mathrm{y}})\rangle$ denotes a function for strain rate sensitivity, f_{y} is the yield function, f_{p} is the plastic potential function, Φ_1 denotes a function for rate sensitivity, and Φ_2 controls the failure state where deviatoric strain becomes infinite.

Based on the experimental results of strain-rate constant triaxial tests (Adachi et al., 1987; Oka et al., 1994), Φ_1 is defined as

$$\Phi_1(f_{\mathrm{y}}) = \exp(m' f_{\mathrm{y}}) \tag{11}$$

where m' is the viscoplastic parameter for a given degree of rate sensitivity.

Yield function f_{y} with two kinematic hardening parameters, namely, x^*_{ij} and y^*_{m}, is given by

$$f_{\mathrm{y}} = \bar{\eta}^*_x + \tilde{M}^*\left(\ln\frac{\sigma'_{\mathrm{m}}}{\sigma'_{\mathrm{ma}}} - y^*_{\mathrm{m}}\right) = 0 \tag{12}$$

$$\bar{\eta}^*_x = \{(\eta^*_{ij} - x^*_{ij})(\eta^*_{ij} - x^*_{ij})\}^{1/2}, \quad \eta^*_{ij} = \frac{S_{ij}}{\sigma'_{\mathrm{m}}} \tag{13}$$

where σ'_{ma} is taken as the initial value of the mean effective stress.

Herein, two strain-hardening parameters are used in the model, namely, x^*_{ij}, which depends on the viscoplastic shear strain rate, and y^*_{m}, which is related to volumetric viscoplastic strain ε^{vp}_{kk}.

The evolutional equations of x^*_{ij} and y^*_{m} are given by

$$\mathrm{d}x^*_{ij} = B^*_1\left(A^*_1\mathrm{d}e^{vp}_{ij} - x^*_{ij}\mathrm{d}\gamma^p\right) \tag{14}$$

$$\mathrm{d}e^{vp}_{ij} = \mathrm{d}\varepsilon^{vp}_{ij} - \frac{1}{3}\mathrm{d}\varepsilon^{vp}_{kk}\delta_{ij}, \quad \mathrm{d}\gamma^p = \sqrt{\mathrm{d}e^{vp}_{ij}\mathrm{d}e^{vp}_{ij}} \tag{15}$$

$$\mathrm{d}y^*_{\mathrm{m}} = \mathrm{d}y^*_{\mathrm{m1}} + \mathrm{d}y^*_{\mathrm{m2}} \tag{16}$$

$$\mathrm{d}y^*_{\mathrm{m1}} = B^*_2\left(A^*_2\mathrm{d}\varepsilon^{vp}_{kk} - y^*_{\mathrm{m1}}|\mathrm{d}\varepsilon^{vp}_{kk}|\right) \tag{17}$$

$$\mathrm{d}y^*_{\mathrm{m2}} = \frac{1+e}{\lambda-\kappa}\mathrm{d}\varepsilon^{vp}_{kk} \tag{18}$$

where A^*_1, A^*_2, A^*_3, B^*_1, and B^*_2 are material parameters and $A^*_1(=M^*_{\mathrm{f}})$ is the value of η^* at the failure state.

A second material function, Φ_2, that is dependent on the internal state variables, is chosen to control the failure state. Basically, it is assumed that Φ_2 becomes infinite at failure (Adachi et al., 1987, 1990), i.e.

$$\Phi_2(\xi) = 1 + \xi \tag{19}$$

in which ξ is an internal variable.

In general, ξ follows an evolutional equation whose integrated form, satisfying the above-mentioned failure requirement for the internal variable, is given by

$$\xi = \frac{M^*_{\mathrm{f}}\bar{\eta}^{**}_{x(0)}}{G^*_2\left\{M^*_{\mathrm{f}} - \frac{\eta^{**}_{mn}(\eta^{**}_{mn}-x^*_{mn})}{\bar{\eta}^{**}_x}\right\}} \tag{20}$$

where G^*_2 is a parameter for the second material function and M^*_{f} is the value of the stress invariant ratio at failure and

$$\bar{\eta}^{**}_x = \{(\eta^{**}_{ij} - x^*_{ij})(\eta^{**}_{ij} - x^*_{ij})\}^{1/2}, \quad \eta^{**}_{ij} = \frac{S^*_{ij}}{\sigma'^*_{\mathrm{m}}} \tag{21}$$

$$\bar{\eta}^{**}_{x(0)} = \{(\eta^{**}_{ij} - x^*_{ij(0)})(\eta^{**}_{ij} - x^*_{ij(0)})\}^{\frac{1}{2}} \tag{22}$$

where η^{**}_{ij} is the stress history invariant ratio, S^*_{ij} and σ'^*_{m} are the deviatoric and the mean components of stress history tensor σ^*_{ij}, respectively, and $x^*_{ij(0)}$ denotes the initial value of x^*_{ij}.

Furthermore, stress history tensor σ^*_{ij} is defined as

$$\sigma^*_{ij} = \frac{1}{\tau}\int_0^z \exp\left(-(z-z')/\tau\right)\sigma_{ij}(z')\mathrm{d}z', \quad 0 \leqslant z' < z \tag{23}$$

$$z = \int_0^t \mathrm{d}z', \quad \mathrm{d}z' = \sqrt{\mathrm{d}e_{ij}\mathrm{d}e_{ij}} \tag{24}$$

where t is time, $\mathrm{d}e_{ij}$ is the increment of deviatoric strain, and τ is a material parameter.

The stress history tensor was advocated by Oka (1985) and Adachi and Oka (1995). In their theory, both the yield and the hardening functions depend on the stress history rather than on the real stress in order to describe the strain-softening behavior of geomaterials. From the assumption that the second material function, Φ_2, is a function of stress history ratio tensor η^{**}_{ij}, it becomes possible to describe the material behavior in which the stress path can reach a point over the failure line. This type of behavior is dominant for overconsolidated clay as was revealed in the experiments (see, for example, Fig. 2).

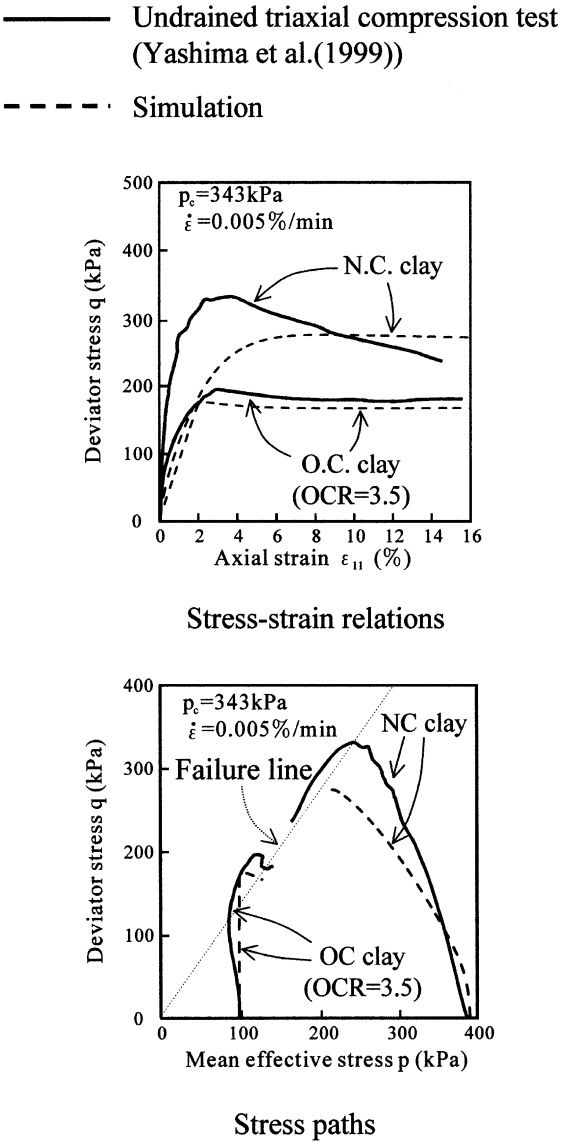

Fig. 2. Stress–strain relations and stress paths of Osaka Pleistocene clay (Yashima et al., 1999).

The plastic potential is given by Eq. (25), which is similar to the yield function, in other words,

$$f_p = \bar{\eta}_x^* + \widetilde{M}^* \left(\ln \frac{\sigma'_m}{\sigma'_{mp}} - y_m^* \right) = 0 \tag{25}$$

$$\bar{\eta}_x^* = \{(\eta_{ij}^* - x_{ij}^*)(\eta_{ij}^* - x_{ij}^*)\}^{\frac{1}{2}}, \quad \eta_{ij}^* = \frac{S_{ij}}{\sigma'_m} \tag{26}$$

$$f_b < 0; \quad \widetilde{M}^* = -\frac{\bar{\eta}^*}{\ln(\sigma'_m/\sigma'_{mc})} \tag{27}$$

$$f_b \geqslant 0; \quad \widetilde{M}^* = M^*_m \tag{28}$$

where f_b is the OC boundary surface given by Eq. (4), and σ'_{mp} is a material parameter, herein taken to be equal to the initial value of σ'_m.

Using the flow rule and the plastic potential function, we obtain the deviatoric viscoplastic strain rates $\dot{e}^{vp}_{ij}$ and volumetric viscoplastic strain rate $\dot{\varepsilon}^{vp}_{kk}$ as:

$$\dot{e}^{vp}_{ij} = C_{01} \exp\left\{ m'\left(\bar{\eta}^*_x + \widetilde{M}^*\left(\ln\frac{\sigma'_m}{\sigma'_{ma0}} - y^*_m \right) \right) \right\} \Phi_2(\xi) \frac{(\eta^*_{ij} - x^*_{ij})}{\bar{\eta}^*_x} \tag{29}$$

$$\dot{\varepsilon}^{vp}_{kk} = C_{02} \exp\left\{ m'\left(\bar{\eta}^*_x + \widetilde{M}^*\left(\ln\frac{\sigma'_m}{\sigma'_{ma0}} - y^*_m \right) \right) \right\} \Phi_2(\xi) \left\{ \widetilde{M}^* - \frac{\eta^*_{mn}(\eta^*_{mn} - x^*_{mn})}{\bar{\eta}^*_x} \right\} \tag{30}$$

From Eq. (30), it is seen that the sign of the volumetric inelastic strain rate depends on the stress state even inside the OC boundary surface, because the volumetric strain depends on the value of $\widetilde{M}^*$ given by Eqs. (27) and (28), and inside the OC boundary surface, $\widetilde{M}^*$ is a function of σ'_{mc} defined by Eq. (7), which is related to the shape of OC boundary surface shown in Fig. 1.

Figs. 3 and 4 show the stress–strain relations and the stress paths under undrained triaxial compression conditions. Table 1 lists the 16 material parameters, including two parameters of the initial conditions, that were used in the analysis in which a linear kinematic hardening equation is assumed for changes in the mean effective stress. Three parameters are different for overconsolidated and normally consolidated clays. This means that the magnitude of strain softening and kinematic hardening depends on the magnitude of OC. Following the tradition of soil mechanics, compression is denoted as positive in the table and in the figures. Both the strain rate effect and the strain-softening behavior are observed in Figs. 3 and 4. From the stress paths, it is seen that the mean effective stress increases due to positive dilatancy for overconsolidated clay, while the mean effective stress decreases due to negative dilatancy for normally consolidated clay. The simulated results qualitatively capture typical stress–strain characteristics of natural clays such as the behavior of stiff Osaka Pleistocene clay shown in Fig. 2 (see Yashima et al. (1999)). From a quantitative point of view, a more thorough study on the determination of the soil parameters for natural clay is necessary to improve the simulated results.

3. Instability of the model

Oka et al. (1995) studied the instability of the viscoplastic model in terms of undrained creep failure for normally consolidated clay. In order to discuss the instability of the proposed viscoplastic model, we herein consider the response of the model under conventional triaxial undrained creep conditions (see Fig. 5) using the same method by Oka et al. (1995). Under undrained creep conditions, a constant deviatoric stress is maintained, although the mean effective stress may change due to the undrained condition that requires a total of zero for the volumetric strain rate.

Under the axisymmetric triaxial testing conditions ($\sigma'_{11} > \sigma'_{22} = \sigma'_{33}$, $\sigma'_{ij} = 0$ $(i \neq j)$), the deviator stress is expressed by q which is defined as

$$q = \sigma'_{11} - \sigma'_{22} \tag{31}$$

Since the total volumetric strain is zero, the following relation is obtained after integration, i.e.

$$\varepsilon^{vp}_{kk} = -\frac{\kappa}{(1+e)} \ln\frac{\sigma'_m}{\sigma'_{me}} \tag{32}$$

where σ'_{me} is the initial value of the mean effective stress.

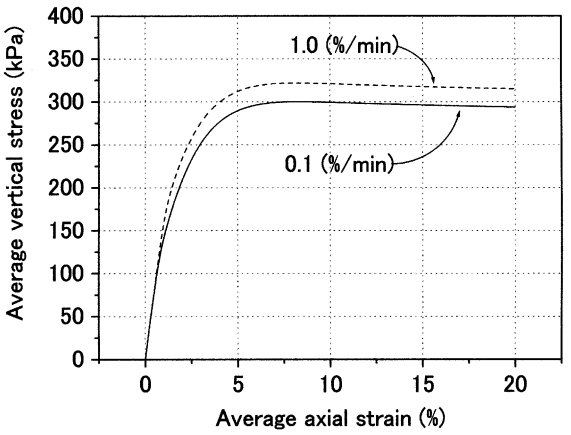

(a) Stress-strain relations (N.C. clay)

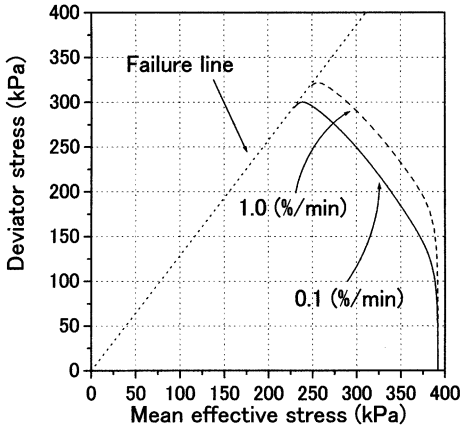

(b) Stress paths (N.C. clay)

Fig. 3. Stress–strain relations and stress paths of NC clay.

Herein, the following variables are used under the triaxial conditions:

$$\eta = \sqrt{3/2}\eta^* = q/\sigma'_{\mathrm{m}}, x_{11} = \sqrt{3/2}x^*_{11} \tag{33}$$

For simplicity, we assume that $M_{\mathrm{f}} = M_{\mathrm{m}} = M$ ($M_{\mathrm{f}} = \sqrt{3/2}M^*_{\mathrm{f}}$, $M_{\mathrm{m}} = \sqrt{3/2}M^*_{\mathrm{m}}$).

Under undrained triaxial conditions, and disregarding the deviatoric elastic strain rate, viscoplastic axial strain rate $\dot{\varepsilon}^{vp}_{11}$ becomes

$$\dot{\varepsilon}^{vp}_{11} = C\Phi_2 \exp\left[m'\left(\frac{1}{M}(\eta - x) + \ln \sigma_{\mathrm{m}}/\sigma'_{\mathrm{me}} - A_3 y_{\mathrm{m}}\right)\right] \tag{34}$$

where A_3 is the volumetric hardening parameter given by $A_3 = (1+e)/(\lambda - \kappa)$.

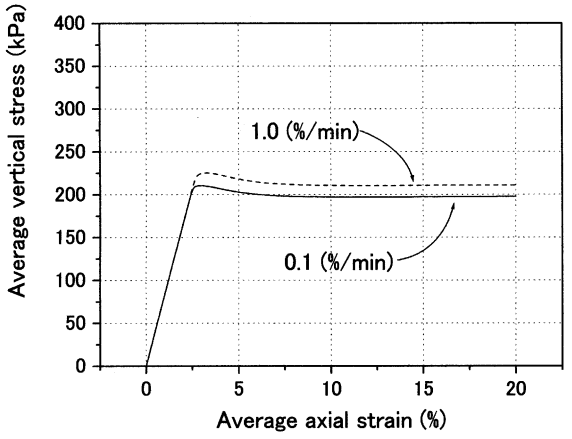

(a) Stress-strain relations (O.C. clay)

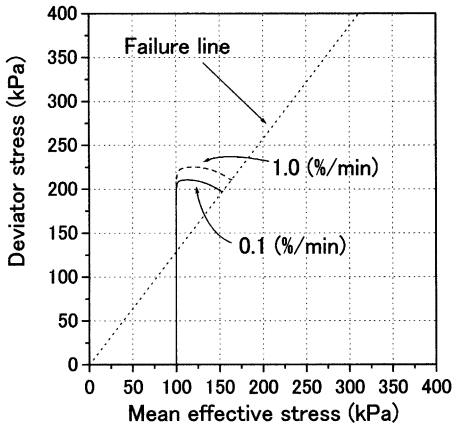

(b) Stress paths (O.C. clay)

Fig. 4. Stress–strain relations and stress paths of OC clay.

Finally, the evolutional equations for the two hardening parameters, x_{11} and y_{m}, are given by

$$\dot{x}_{11} = B(A - x_{11})\dot{\varepsilon}_{11}^{vp} \tag{35}$$

$$\dot{y}_{\mathrm{m}} = \dot{y}_{\mathrm{m2}} = A_3\dot{\varepsilon}_{kk} \tag{36}$$

where $B = \sqrt{3/2}B^*$, $A = \sqrt{3/2}A^* = M_{\mathrm{f}}$, and $y_{\mathrm{m1}} = 0$.

Let us calculate a rate of strain rate denoted by $\ddot{\varepsilon}_{11}^{vp}$. By examining the sign of the rate of strain rate $\ddot{\varepsilon}_{11}^{vp}$, we can estimate the stability of the material system. For example, if the rate of strain rate is positive, the material undergoes a creep failure.

Table 1
Material parameters used in the calculations

Parameter	NC clay	OC clay
Compression index (λ)	0.172	0.172
Swelling index (κ)	0.054	0.054
Initial void ratio (e_0)	0.72	0.72
Initial mean effective stress (σ'_{me})	392 (kPa)	100 (kPa)
Parameter of OC boundary surface (σ'_{mbi})	392 (kPa)	392 (kPa)
Coefficient of earth pressure at rest[a] (K_0)	1.0	1.0
Viscoplastic parameter (m')	21.5	21.5
Viscoplastic parameter (C_{01})	4.5×10^{-8} (1/s)	4.5×10^{-8} (1/s)
Viscoplastic parameter (C_{02})	4.5×10^{-8} (1/s)	4.5×10^{-8} (1/s)
Stress ratio at failure (M_f^*)	1.05	1.05
Stress ratio at maximum compression (M_m^*)	1.05	1.05
Elastic shear modulus (G)	5500 (kPa)	5500 (kPa)
Softening parameter (G_2^*)	100	1
Kinematic hardening parameter (B_1^*)	0.0	0.5
Kinematic hardening parameter[b] (A_2^*)	0.0	0.0
Kinematic hardening parameter[b] (B_2^*)	0.0	0.0
Retardation parameter (τ)	1.0×10^{-3}	0.2
Coefficient of permeability[a] ($k_x = k_y$)	1.54×10^{-6} (m/s)	1.54×10^{-6} (m/s)
	1.54×10^{-8} (m/s)	1.54×10^{-8} (m/s)
	1.54×10^{-10} (m/s)	1.54×10^{-10} (m/s)

[a] K_0 and coefficient of permeability were used in finite element analysis.
[b] A_2^* and B_2^* were not used in the present analysis.

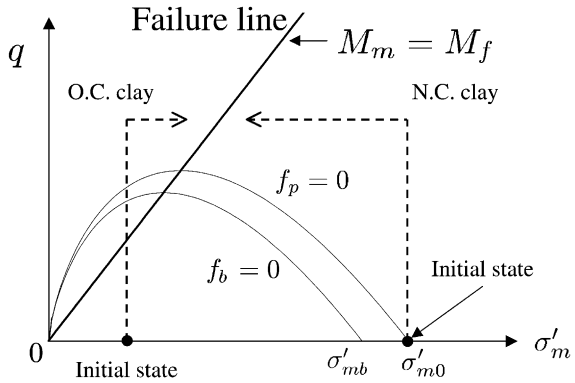

Fig. 5. Stress paths of undrained creep for NC and OC clays.

Upon time differentiation of a viscoplastic strain rate without a second material function, the rate of strain rate is obtained as

$$\ddot{\varepsilon}_{11} = -m'(\dot{\varepsilon}_{11}^{vp})^2\left[\frac{1+e}{M\kappa}(\eta - M)\left(\eta - \frac{\lambda}{\lambda-\kappa}M\right) + \frac{B}{M}(A - x_{11})\right] = -m'a(\dot{\varepsilon}_{11}^{vp})^2 \tag{37}$$

$$a = \left[\frac{1+e}{M\kappa}(\eta - M)\left(\eta - \frac{\lambda}{\lambda-\kappa}M\right) + \frac{B}{M}(A - x_{11})\right] \tag{38}$$

In the above derivation, the stress dilatancy relation

$$\frac{\dot{\varepsilon}_{kk}^{vp}}{\dot{\varepsilon}_{11}^{vp}} = M - \eta$$

and the undrained condition

$$\dot{\varepsilon}_{kk}^{vp} = -\frac{\kappa}{1+e}\frac{\dot{\sigma}'_{\mathrm{m}}}{\sigma'_{\mathrm{m}}}$$

are introduced.

We will discuss the instability of the model using Eqs. (37) and (38) and the assumption that the last term is small, since $A - x_{11} \approx 0$ near the failure state. Firstly, we consider the case of undrained creep for normally consolidated clay in which $\eta < M$. In this case, the following conditions prevail, namely, $M - \eta > 0$, $(\frac{\lambda}{\lambda-\kappa}M - \eta) > 0$, and $A - x_{11} > 0$. Since $a > 0$, the rate of strain rate is negative, which leads to the conclusion that the material system is structurally stable in terms of Liapunov.

Next, we will consider the second material function for normally consolidated clay. The second material function is simplified with the assumption that the initial value of $x_{11(0)}$ is zero; i.e., $x_{11} = 0$. Thus,

$$\Phi_2 = 1 + \frac{M\eta}{G_2(M-\eta)} = \frac{G_2(M-\eta) + M\eta}{G_2(M-\eta)} \tag{39}$$

in which $G_2 = \sqrt{2/3}G_2^*$.

$$\begin{aligned}\ddot{\varepsilon}_{11} &= -m'(\dot{\varepsilon}_{11}^{vp})^2\left[-\frac{(1+e)M^2\eta}{m'\kappa(G_2(M-\eta)+M\eta)} + \frac{1+e}{M\kappa}(\eta - M)\left(\eta - \frac{\lambda}{\lambda-\kappa}M\right) + \frac{B}{M}(A_3 - x)\right] \\ &= -m'a(\dot{\varepsilon}_{11}^{vp})^2 \end{aligned} \tag{40}$$

In contrast to the case without a second material function, it is found that when a second material function is included, the rate of strain rate $\ddot{\varepsilon}_{11}^{vp}$ may become positive before η reaches M, since the first term in the square brackets of Eq. (40) increases with a negative sign. Hence, the introduction of a second material function is inevitable for describing the creep failure of normally consolidated clay in the case of monotonically increasing hardening function (see Fig. 6). This is consistent with previous results of tests on the instability of normally consolidated clay obtained by Adachi et al. (1990), Oka et al. (1995).

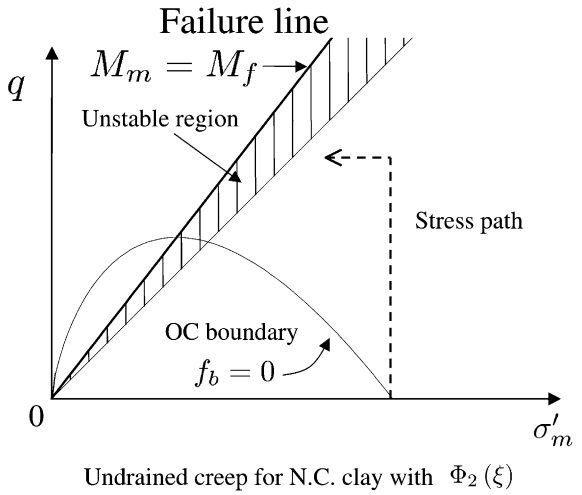

Fig. 6. Unstable region of NC clay under undrained conditions.

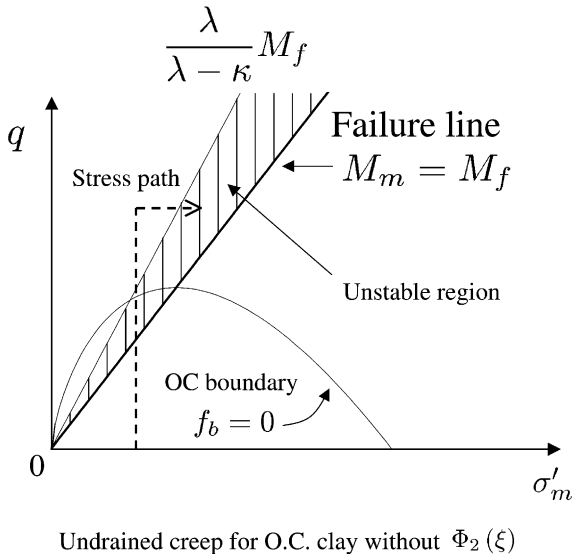

Fig. 7. Unstable region of OC clay under undrained conditions without a second material function.

Next, we will discuss the stability of the model in the region where $\eta > M$. This condition corresponds to the undrained creep tests which can be achieved by applying deviator stress q with a small initial mean effective stress located in the overconsolidated region. When there is no second material function, the term a becomes positive in region $M < \eta < \lambda/(\lambda - \kappa)M$, as shown in Fig. 7. In this region, the material becomes unstable due to the fact that $\dot{\varepsilon}_{11}^{vp} > 0$. On the other hand, when second material function Φ_2 is introduced, the stability cannot be evaluated with Eq. (40) in the region where $\eta > M$ because $\xi(=(M\eta)/[G_2(M-\eta)])$ becomes negative due to a simplification which involves the replacement of η_{ij}^{**}, defined by the stress history tensor, with η_{ij}^{*} based on the stress tensor.

From the above considerations, it becomes evident that the model can simulate the instability associated with "undrained creep failure" in the specific stress regions. It is worth noting that in the region where $\eta > M$, the model can be unstable even if a second material function is not included.

Using an isotropic hardening viscoplastic model, Oka et al. (1994) found that the material model developed by Adachi and Oka (1982) is always stable without a second material function, i.e. $\Phi_2 = 1$ in the normally consolidated region. From the above consideration, however, it becomes evident that overconsolidated clay becomes unstable in region ($\eta > M$) even for models without a second material function.

4. Finite element analysis of strain localization by an elasto-viscoplastic model

Oka et al. (1994, 1995) numerically studied the strain localization problem using an elasto-viscoplastic model for normally consolidated clay based on a Perzyna type of overstress model and a Cam-clay model. They found that strain localization is closely linked to material instability, and can be simulated with a viscoplastic softening model. In previous studies, a model which can reproduce only negative dilatancy, such as in the case of normally consolidated clays, was used. On the other hand, it is well known that overconsolidated clay exhibits positive dilatancy, i.e. a volume increase during shear deformation. In this section, the effects of dilatancy and permeability on strain localization are numerically studied using the model proposed in the previous section.

Numerical solutions for the plane strain compression problems of water-saturated clay are obtained via the finite element method. In the finite element analysis, the updated Lagrangian method with the objective Jaumann rate of Cauchy stress is used for a weak form of the equilibrium equation (see Oka et al., 2000a,b).

Nominal stress rate tensor $\dot{\mathbf{S}}$ is given by

$$\dot{\mathbf{S}} = \dot{\mathbf{T}} + \mathrm{tr}\mathbf{L}\mathbf{T} - \mathbf{T}\mathbf{L}^{\mathrm{T}} \tag{41}$$

$$\dot{\mathbf{S}}' = \dot{\mathbf{T}}' + \mathrm{tr}\mathbf{L}\mathbf{T}' - \mathbf{T}'\mathbf{L}^{\mathrm{T}} \tag{42}$$

where $\mathbf{T}$ is the Cauchy stress tensor, $\mathbf{T}' = \mathbf{T} - u_w\mathbf{I}$ is the effective Cauchy stress tensor, $\mathbf{L}$ is the velocity gradient tensor, the superposed dot denotes time differentiation, tr is the trace operator, $\mathbf{T}'$ is the effective Cauchy stress tensor, $\dot{\mathbf{S}}'$ is the effective nominal stress tensor, and $\mathbf{I}$ is the second order identity tensor.

The weak form of the equilibrium equation for the whole fluid–solid mixture is

$$\int_v S_{ji,j}\delta v_i \,\mathrm{d}V = 0 \tag{43}$$

where v_i is the component of the velocity vector.

For describing the motion of pore water, a Biot type of two-phase mixture theory (Biot, 1956) is used in the analysis with a v_i(velocity) $- u_w$(pore pressure) formulation, i.e.

$$\frac{k}{\gamma_w}u_{w,ii} + D_{ii} = 0 \tag{44}$$

where γ_w is the unit weight of the pore fluid and D_{ij} is the stretching tensor.

In the analysis, D_{ij} is used instead of $\dot{\varepsilon}_{ij}$ when writing the constitutive equations. For the stress rate tensor in the model, the Jaumann rate of Cauchy stress tensor $\widehat{\mathbf{T}}$ is adopted as the objective tensor, namely,

$$\widehat{\mathbf{T}} = \dot{\mathbf{T}} - \mathbf{W}\mathbf{T} + \mathbf{T}\mathbf{W} \tag{45}$$

where $\mathbf{W}$ is the spin tensor.

The elasto-viscoplastic constitutive model is written as

$$\widehat{\mathbf{T}}' = \mathbf{C}\mathbf{D} - \mathbf{Q} \tag{46}$$

where $\mathbf{C}$ is the tangential stiffness tensor and $\mathbf{Q}$ is the relaxation stress tensor.

In the finite-element formulation, the tangent modulus method (Pierce et al., 1984) is used. An eight-node quadrilateral element with a reduced Gaussian (2×2) integration (see Fig. 8) is used to eliminate the shear locking and to reduce the appearance of a spurious hourglass mode. On the other hand, the pore water pressure is defined at four corner nodes. A weak form of the continuity equation is integrated with a (2×2) full integration (see Fig. 8). Using this combination of the spatial integration scheme, the effective stresses, the pore water pressure, and the strain are all calculated at the same integration points for each element.

Fig. 9 shows the size of the specimen and the associated boundary conditions. As a trigger for strain localization, horizontal displacements on both top and bottom surface edges are constrained. Relaxation of this constraint through the introduction of a frictional boundary will be discussed later. The material parameters used in the analysis are listed in Table 1 with the coefficient of permeability and the K_0 values. In the analysis, the time increment is determined by the increment of average strain $\Delta\varepsilon_{11} = 0.01\%$. In this case, a time increment of 6 s is used.

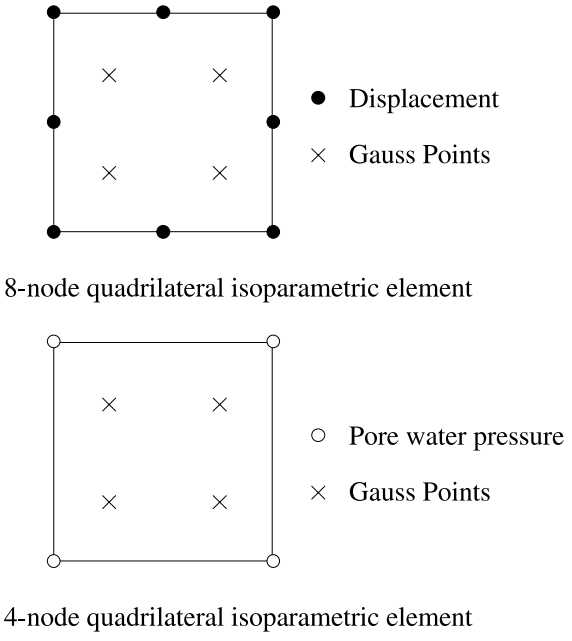

Fig. 8. Finite elements and Gauss integration points.

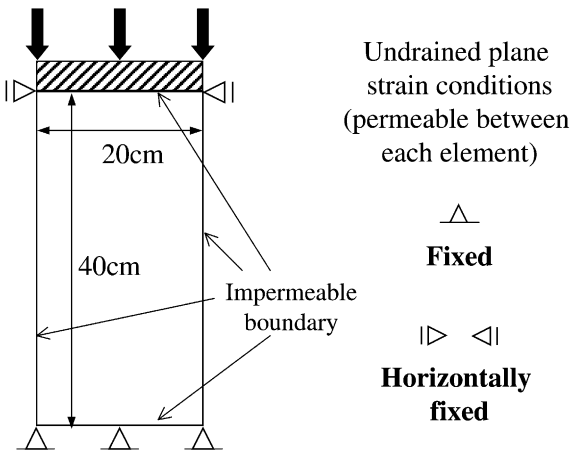

Fig. 9. Size of specimen and boundary conditions.

4.1. Effects of dilatancy

The compression of a clay specimen is simulated under globally undrained plane strain conditions. Compression is performed under displacement control with average strain rates of 0.1%/min and 1%/min. Fig. 10 shows the average stress–strain relationships; it is clearly seen that the strain rate influences the

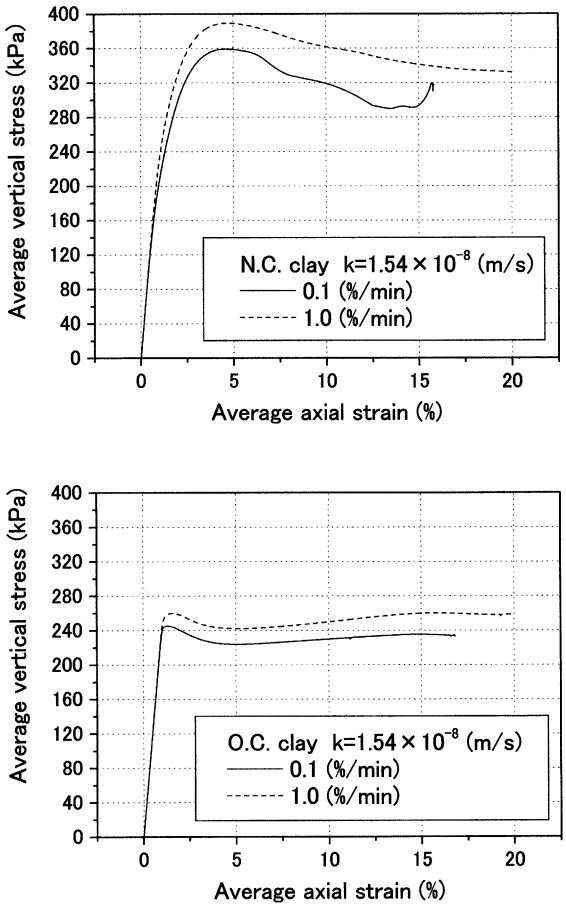

Fig. 10. Average stress–strain relations.

associated stress–strain responses. Fig. 11 shows the simulated results for normally consolidated and overconsolidated clays with a permeability coefficient of 1.54×10^{-8} (m/s).

It can be seen from Fig. 11 that the deformed meshes of normally and overconsolidated clay specimens display localization of deformation at an average axial strain of 8% and 6%, respectively. The appearance of the shear band at a larger strain in NC clay is consistent with the stress–strain curves with gradual softening. The occurrence of localization at an early stage of deformation in the case of overconsolidated clay is consistent with the average stress–strain relationships shown in Fig. 10. This tendency has been observed in the experiments (e.g. Hicher et al., 1994).

Fig. 12 shows the accumulated viscoplastic shear strain $\gamma^p \equiv \int \sqrt{\mathrm{d}e_{ij}^{vp}\mathrm{d}e_{ij}^{vp}}$. In the case of overconsolidated clay, strain localization starts near the edges of the top and the bottom plates, and finally, four shear bands appear. In contrast to the case of overconsolidated clay, only two shear bands are seen for normally consolidated clay, with shear bands clearly developing just beneath the edges of the top and the bottom plates. As for the distribution of viscoplastic volumetric strain magnitude, it is seen from Fig. 13 that a decrease in viscoplastic volumetric strain (viscoplastic volume expansion) occurs along the shear bands for overconsolidated clay, while only viscoplastic compression is seen in the case of normally consolidated clay. The tendency of the distribution of viscoplastic volumetric strain is, in fact, related to the changes in mean

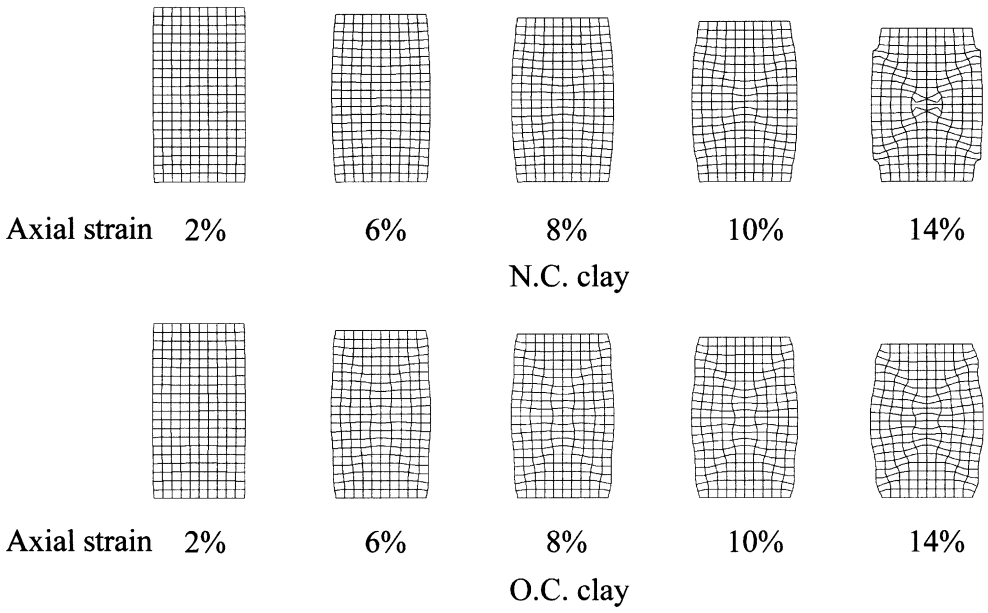

Fig. 11. Deformed meshes of NC and OC clays ($\dot{\varepsilon}_{11} = 0.1\%$/min, $k = 1.54 \times 10^{-8}$ m/s).

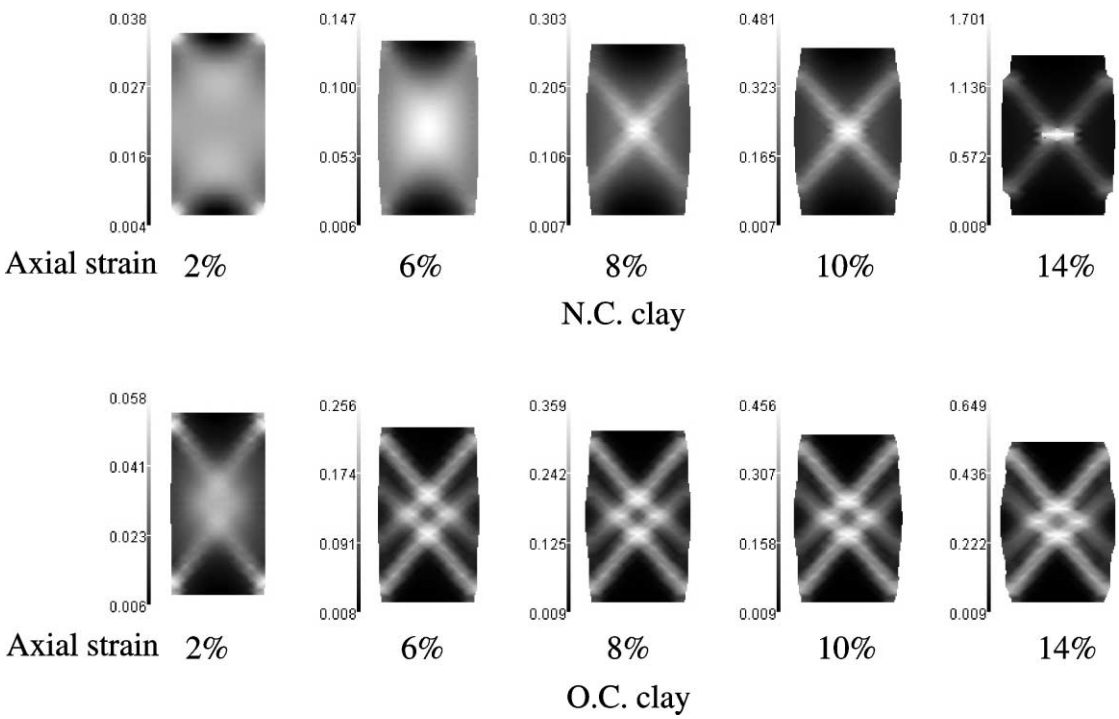

Fig. 12. Distribution of γ^p for NC and OC clays ($\dot{\varepsilon}_{11} = 0.1\%$/min, $k = 1.54 \times 10^{-8}$ m/s).

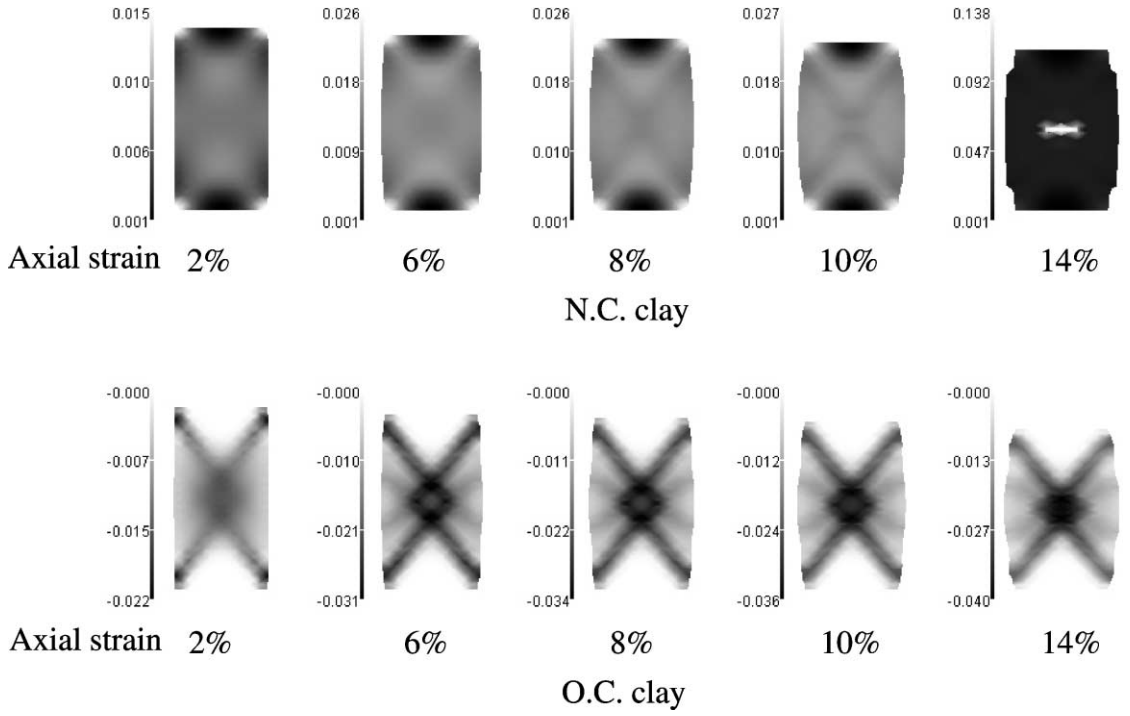

Fig. 13. Distribution of accumulated viscoplastic volumetric strain for NC and OC clays ($\dot{\varepsilon}_{11} = 0.1\%/\text{min}$, $k = 1.54 \times 10^{-8}$ m/s).

effective stresses since calculations are carried out under globally undrained conditions. Fig. 14 shows the distribution of mean effective stress with the progress of average axial strain. In the case of overconsolidated clay, the mean effective stress generally increases in the specimen from its initial value, i.e. 100 kPa. However, along the shear bands, mean effective stress levels are lower than those in the other regions of the specimen. In the case of normally consolidated clay, the mean effective stress decreases from its initial value of 392 kPa due to negative dilatancy. The extent of the decrease in mean effective stress is larger in shear bands.

In general the distribution of mean effective stress is related to pore fluid motion. Hence, in order to examine the distribution of mean effective stress, it is necessary to evaluate the effect of the permeability coefficient. Fig. 15 shows the distributions of mean effective stress and viscoplastic volumetric strain for overconsolidated clay with a permeability coefficient as low as 1.54×10^{-10} (m/s). In this case, the mean effective stress along the shear bands is relatively higher than that in the regions between them. This tendency is in contrast to that found in the numerical results obtained for the high permeability case shown in Fig. 14. The reason for this difference is that pore water can easily move within a material with high permeability. Hence, an increase in mean effective stress due to positive dilatancy can be cancelled by the inflow of pore water toward the shear bands. Fig. 16 displays the distribution of pore water pressure. Comparing the distributions of mean effective stress and plastic shear strain, it is seen that the distribution of pore water pressure is rather homogeneous for both normally and overconsolidated clays. However, higher levels of pore water pressure develop for normally consolidated clay. The relatively homogeneous distribution of pore water pressure within the specimen is considered to be due to the migration of pore water.

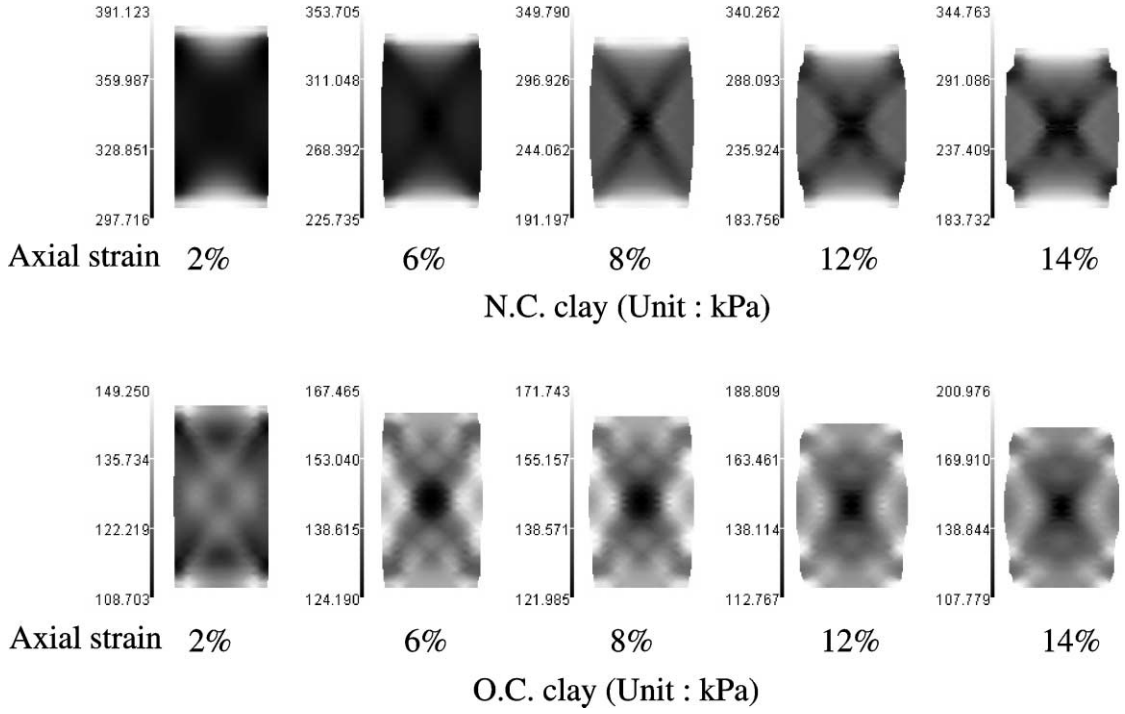

Fig. 14. Distribution of mean effective stress for NC and OC clays ($\dot{\varepsilon}_{11} = 0.1\%$/min, $k = 1.54 \times 10^{-8}$ m/s).

4.2. Effects of strain rate and permeability

The deformed meshes for higher average strain rates (1%/min) are shown in Fig. 17. It is seen that normally consolidated clay is more stable with higher strain rates, while the effect of strain rates is not very significant for overconsolidated clay. The reason for this observation is that, for normally consolidated clay, the mean effective stress greatly changes before the peak stress owing to the shape of the plastic potential function. This is not the case for overconsolidated clay. Fig. 18 displays the distribution of accumulated viscoplastic shear strain γ^p with different permeability coefficients. In Fig. 16, the appearance of four shear bands is clearly seen for the cases of lower permeability levels. In addition, the figure shows that the distance between the shear bands is wider than that in the case of higher permeability levels. A possible reason for the larger number of shear bands in the overconsolidated clay than in the normally consolidated clay is that the strain softening associated with dilation may cause a reduction in the mean effective stress. Consequently, the adjacent regions can easily deform so as to lead to the occurrence of a larger number of shear bands. The average stress is higher for cases with lower permeability levels ($k = 1.54 \times 10^{-10}$ m/s). As pointed out by Loret and Prevost (1991), materials with low permeability levels are more stable than those with high permeability levels. This tendency of the stress–strain response is similar to the effect of the strain rate.

4.3. Mesh size dependency

In order to check the mesh size dependency of the numerical results, simulations are performed using various mesh sizes. For normally consolidated clay, there is no significant mesh size dependency (Oka et al.,

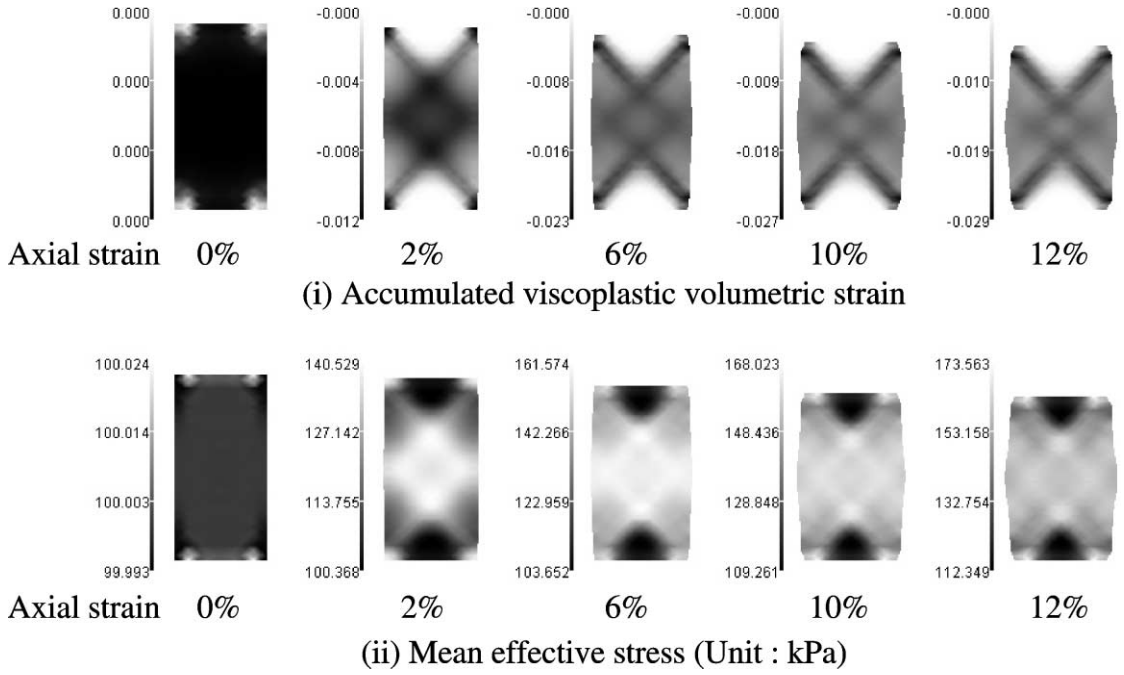

Fig. 15. Distribution of mean effective stress and accumulated viscoplastic volumetric strain for OC clay ($\dot{\varepsilon}_{11} = 0.1\%/\text{min}$, $k = 1.54 \times 10^{-10}$ m/s).

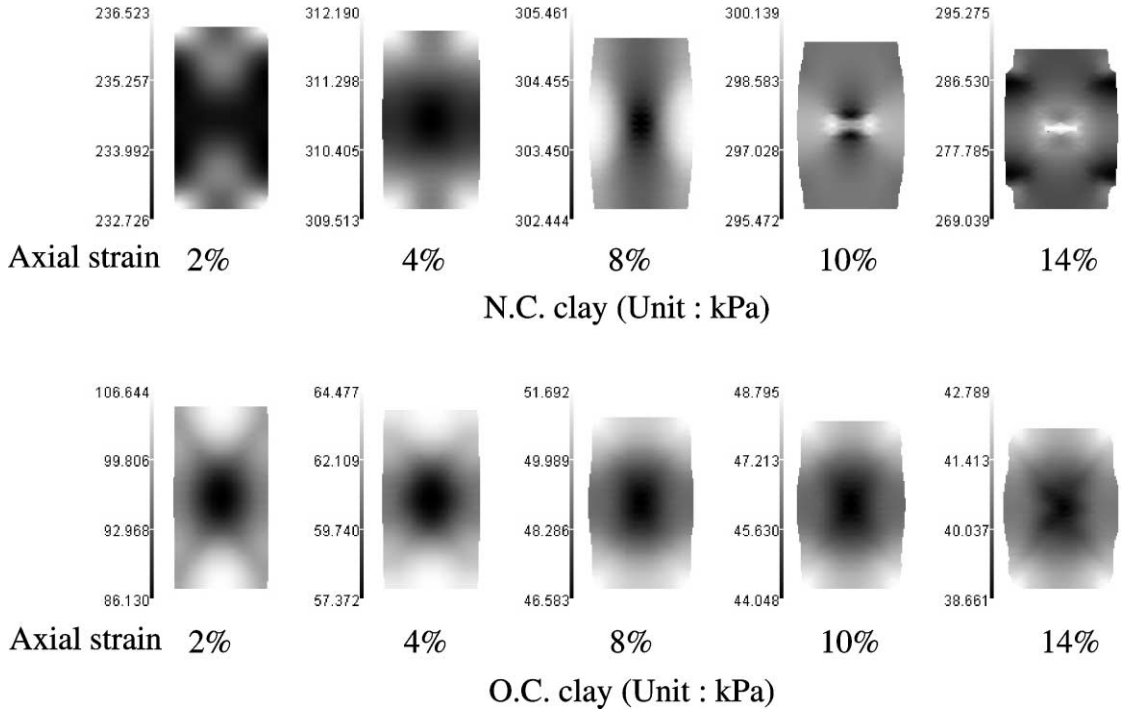

Fig. 16. Distribution of pore water pressure for NC and OC clays ($\dot{\varepsilon}_{11} = 0.1\%/\text{min}$, $k = 1.54 \times 10^{-8}$ m/s).

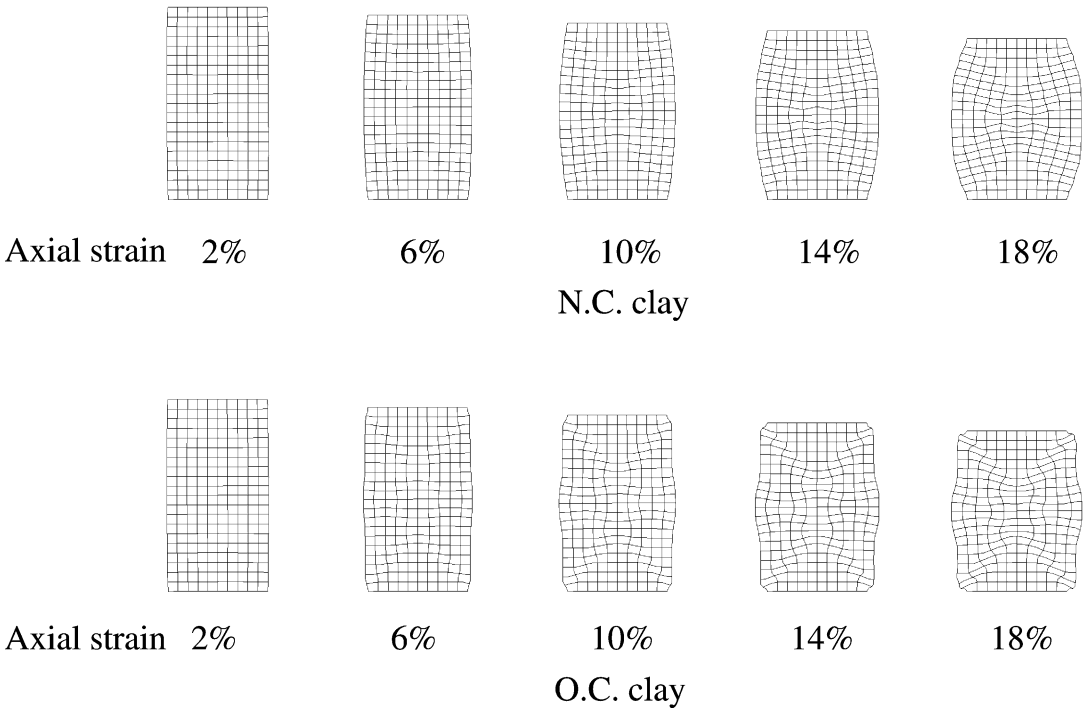

Fig. 17. Deformed meshes of NC and OC clays ($\dot{\varepsilon}_{11} = 1.0\%$/min, $k = 1.54 \times 10^{-8}$ m/s).

1995). As for the overconsolidated clay, numerical calculations with smaller elements (800 elements) diverged after the peak stress around 2% of the axial strain. In order to examine the effect of the end constraints, the "no lateral displacements at top and bottom plates" was relaxed by instead using a frictional boundary with a frictional coefficient of 0.00001. Fig. 19 shows the deformed meshes for different numbers of elements. Since no noticeable mesh size dependency is observed in Fig. 19, the occurrence of any numerical instability can only result from the imposition of strong constraints. No influence of mesh size on stress–strain responses is seen in Fig. 20. Hence, it is worth noting that the numerical calculations for overconsolidated clay are more sensitive to constraint conditions than those for normally consolidated clay. In other words, OC clay easily leads to instability. This tendency is consistent with the results of the instability analysis obtained in Section 3.

5. Conclusions

The main conclusions obtained from this paper are as follows. In the first part of this paper, an elasto-viscoplastic constitutive model for clay was derived based on a Chaboche type of viscoplasticity theory. The proposed model can very well reproduce both positive and negative dilatancy characteristics which are the important characteristics of soil. Next, the instability of the model was studied under undrained triaxial creep conditions for simplicity. It was seen that the model with positive dilatancy was more unstable than the model with negative dilatancy in terms of creep failure. Even when a second material function was not included in the formulation, the model could become unstable with positive dilatancy. On the other hand, the model with negative dilatancy became unstable only when a second material function was introduced.

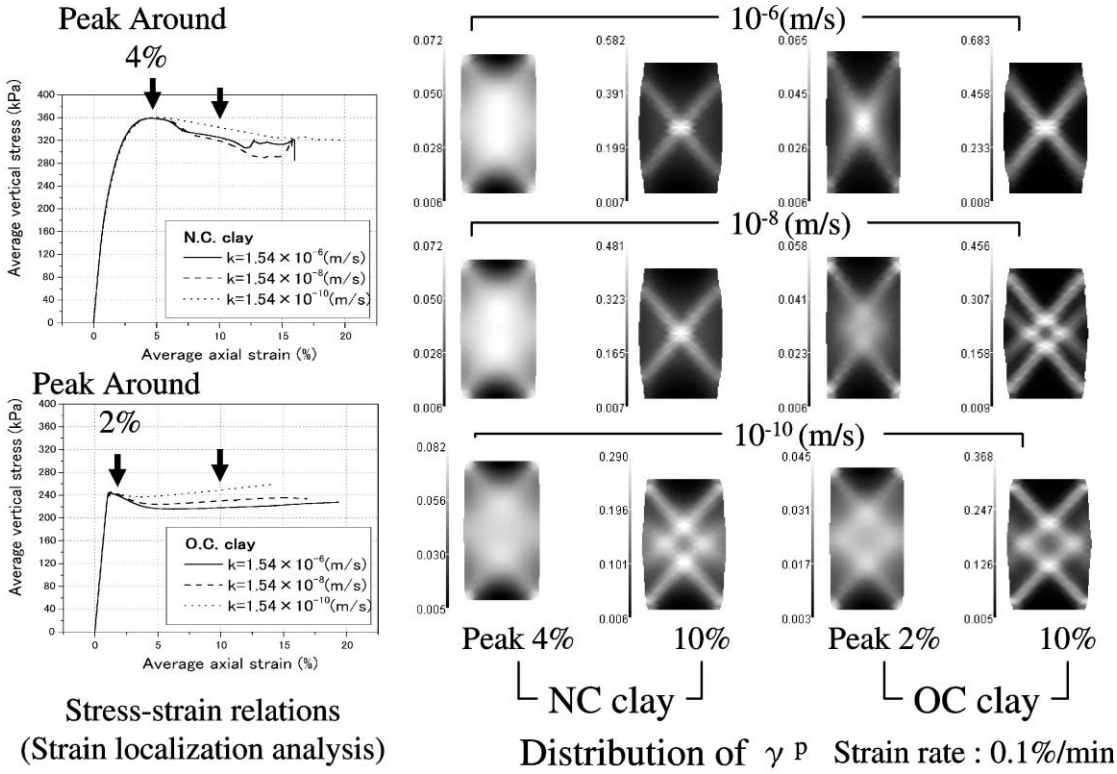

Fig. 18. Distribution of γ^p and stress–strain relations with different permeability coefficients.

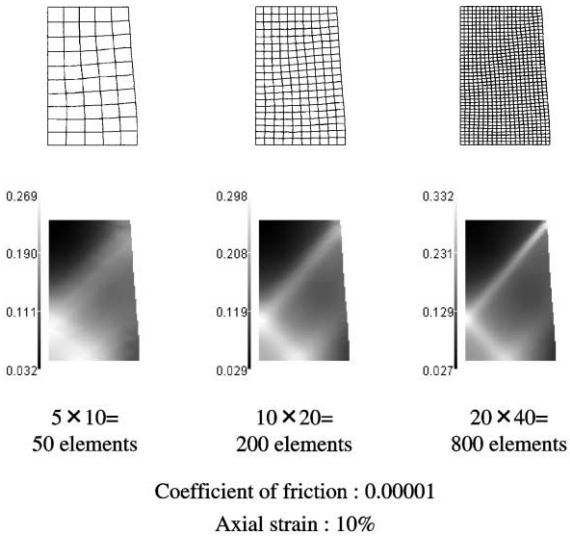

Fig. 19. Deformed mesh and distribution of γ^p for OC clay with different element size ($\dot{\varepsilon}_{11} = 0.1\%/\text{min}$, $k = 1.54 \times 10^{-8}$ m/s).

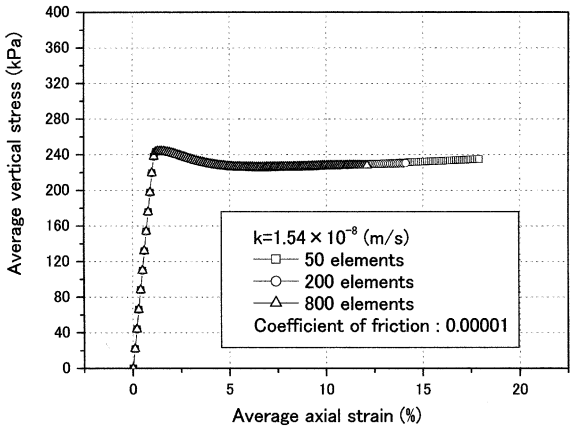

Fig. 20. Average stress–strain relations of OC clay with different element size ($\dot{\varepsilon}_{11} = 0.1\%$/min, $k = 1.54 \times 10^{-8}$ m/s).

As for the numerical simulation of the shear band development, using the elasto-viscoplastic model, it was found that dilatancy characteristics strongly affect the strain localization pattern as well as the permeability and the strain rate.

Acknowledgements

The authors wish to thank the reviewers, Dr. T. Kodaka of Kyoto University and Dr. Richard Wan of the University of Calgary for their fruitful comments.

References

Adachi, T., Oka, F., 1982. Constitutive equations for normally consolidated clay based on elasto-viscoplasticity. Soils and Foundations 22 (4), 57–70.

Adachi, T., Oka, F., 1984. Constitutive equations for sands and overconsolidated clays and assigned works for sand. In: Gudehus, G., Darve, F. (Eds.), Proceedings of International Workshop on Constitutive Relations for Soils, Grenoble, 1982. Balkema, pp. 141–157.

Adachi, T., Oka, F., Mimura, M., 1987. An elasto-viscoplastic theory for clay failure. In: Proceedings of 8th Asian Regional Conference on Soil Mechanics and Foundation Engineering Kyoto, vol. 1. Japanese Society for Soil Mechanics and Foundation Engineering, pp. 5–8.

Adachi, T., Oka, F., Mimura, M., 1990. Elasto-viscoplastic constitutive equations and their application to consolidation analysis. Journal of Engineering Materials and Technology, ASME 112, 202–209.

Adachi, T., Oka, F., 1995. An elasto-plastic constitutive model for soft rock with strain softening. Int. J. Numer. Anal. Meth. Geomech. 19, 233–247.

Aifantis, E.C., 1984. On the microstructural origin of certain inelastic models, ASME. J. Engng. Mater. Tech. 106, 326–330.

Aifantis, E.C., 1987. The physics of plastic deformation. Int. J. Plastic. 3, 211–247.

Aifantis, E.C., Oka, F., Yashima, A., Adachi, T., 1999. Instability of gradient dependent elasto-viscoplasticity for clay. Int. J. Numer. Anal. Meth. Geomech. 23 (10), 973–994.

Biot, M.A., 1956. Theory of propagation of elastic waves in a fluid saturated porous solid. J. Acoust. Soc. Am. 28 (1), 168–191.

Chaboche, J.L., Rousselier, G., 1980. On the plastic and viscoplastic constitutive equations—Part I: Rules developed with internal variable concept. J. Pressure Vessel Tech., ASME 105, 103–158.

Cormeau, I.C., 1975. Numerical stability in quasi-static elasto/viscoplasticity. Int. J. Numer. Meth. Engng. 9, 109–127.

de Borst, R., Sluys, L.J., 1991. Localization in a Cosserat continuum under static and dynamic loading conditions. Comp. Meth. Appl. Mech. Engng. 90, 805–827.

Hicher, P.Y., Wahyudi, H., Tessier, D., 1994. Microstructural analysis of strain localisation in clay. Comput. Geotech. 16, 205–222.
Hughes, T.J.R., Taylor, R.J., 1978. Unconditionally stable algorithms for quasi-static elasto-viscoplastic finite element analysis. Comput. Struct. 8, 169–173.
Hutchinson, J.W., 2001. Strain gradient plasticity theory revisited. In: Material Science for 21st Century, Japan, May 2001, vol. 1A. The Society of Material Science, pp. 307–315.
Loret, B., Prevost, J.H., 1991. Dynamic strain localization in fluid-saturated porous media. J. Engng. Mech., ASCE 117 (4), 907–922.
Mühlhaus, H.-B., Aifantis, E.C., 1991. A variational principle for gradient plasticity. Int. J. Solid. Struct. 28 (7), 845–857.
Oka, F., 1985. Elasto/viscoplastic constitutive equations with memory and internal variables. Comput. Geotech. 1, 59–69.
Oka, F., 1992. A cyclic elasto-viscoplastic constitutive model for clay based on the non-linear-hardening rule. In: Pande, G.N., Pietruszczak, S. (Eds.), Proceedings of 4th International Symposium on Numerical Models in Geomechanics Swansea, vol. 1. Balkema, pp. 105–114.
Oka, F., Adachi, T., Yashima, A., 1994. Instability of an elasto-viscoplastic constitutive model for clay and strain localization. Mech. Mater. 18, 119–129.
Oka, F., Adachi, T., Yashima, A., 1995. A strain localization analysis of clay using a strain softening viscoplastic model. Int. J. Plastic. 11 (5), 523–545.
Oka, F., Yashima, A., Tateishi, A., Taguchi, Y., Yamashita, S., 1999. A cyclic elasto-plastic constitutive model for sand considering a plastic-strain dependence of the shear modulus. Geotechnique 49 (5), 661–680.
Oka, F., Yashima, A., Sawada, K., Aifantis, E.C., 2000a. Instability of gradient-dependent elastoviscoplastic model for clay and strain localization. Comput. Meth. Appl. Mech. Engng. 183, 67–86.
Oka, F., Higo, Y., Jiang, M., 2000b. Effects of material inhomogeneity and transport of pore water on strain localization analysis of fluid-saturated strain gradient viscoplastic geomaterial. In: Khan, A.S., Zhang, H., Yuan, Y. (Eds.), Proceedings of 8th International Symposium on Plasticity and Current Applications, Whistler. Neat Press, pp. 306–308.
Pierce, D., Shih, C.F., Needleman, A., 1984. A tangent modulus method for rate dependent solids. Comput. Struct. 18 (5), 875–887.
Perzyna, P., 1963. The constitutive equations for work-hardening and rate sensitive plastic materials. Proc. Vibrat. Prob., Warsaw 4 (3), 281–290.
Rice, J., 1976. The localization of plastic deformation. In: Koiter, W.T. (Ed.), IUTAM Symposium, Theoretical and Applied Mechanics. Noth-Holland, pp. 207–220.
Rice, J., 1975. On the stability of dilatant hardening for saturated rock masses. J. Geophys. Res. 80 (11), 1531–1536.
Schrefler, B.A., Sanavia, L., Majorana, C.E., 1996. A multiphase medium model for localisation and postlocalisation simulation in geomaterials. Mech. Cohes-Fict. Mater. 1 (1), 95–114.
Simo, J.C., Hughes, T.J.R., 1997. Computational Inelasticity. Springer, Berlin.
Vardoulakis, I., Aifantis, E.C., 1991. A gradient flow theory of plasticity for granular materials. Acta Mech. 87, 197–217.
Yashima, A., Shigematsu, H., Oka, F., Nagaya, J., 1999. Mechanical behavior and micro-structure of Osaka upper-most Pleistocene marine clay. Jou. Geotech. Engng., JSCE 624 (III-47), 217–229 (in Japanese).